Stanford Exploration Project, Report 124, April 4, 2006, pages 1–??

AMO inversion to a common azimuth dataset: Field data results

Robert G. Clapp

ABSTRACT

I cast 3-D data regularization as a least-squares inversion problem. I form a linear operator that maps from irregular dataspace 5-D data space to a regular 4-D common azimuth volume using a cascade of linear interpolation and Azimuth Move-out (AMO) binning. I regularize the inversion by adding minimizes the difference between various $(t, \text{cmp}_x, \text{cmp}_y)$ cubes by applying a filter that acts along offset. AMO is used to transform the cubes to the same hx before applying the filter. Further efficiency is gained by inverting each frequency independently. I apply the methodology on marine dataset and compare the results with two more conventional approaches.

INTRODUCTION

The irregularity of seismic data, particularly 3-D data, in both the model domain (in terms of subsurface position and reflection angle) and the data domain (in terms of midpoint, offset, and time) causes imaging problems. Migration methods desire a greater level of regularity than is often present in seismic surveys. There are two general approaches to deal with this problem. One approach is to treat the imaging problem as an inverse problem. The migration operator can be thought of as a linear transform from the recorded data to image space. Ronen and Liner (2000); Duquet and Marfurt (1999); Prucha et al. (2000) use the migration operator in a linear inverse problem to overcome irregular and limited data coverage. A regularization that encourages consistency over reflection angle is used to stabilize the inverse. These approaches have shown promise but are generally prohibitively expensive, and rely on an accurate subsurface velocity model.

Another approach is to try to regularize the data. AMO provides an effective regularization tool (Biondi et al., 1998) and is generally applied as an adjoint to create a more regularized volume. These regularized volumes still often contain an 'acquisition footprint' or more subtle amplitude effects. Chemingui (1999) used a log-stretch transform to make the AMO operator stationary in time. He then cast the regularization problem as a frequency-by-frequency inversion problem using a Kirchoff-style AMO operator. He showed that the acquisition footprint could be significantly reduced. The downside of this approach is the relatively high cost of Kirchoff implementation of AMO.

Biondi and Vlad (2001) built on the work of Fomel (2001) and set up an inverse problem relating the irregular input data to a regular model space. They regularized the problem by

enforcing consistency between the various $(t, \text{cmp}_x, \text{cmp}_y)$ cubes. The consistency took two forms. In the first, a simple difference between two adjacent in-line offset cubes was minimized. In the second, the difference was taken after transforming the cubes to the same offset AMO. Clapp (2005b) set up the data regularization with AMO as an inverse problem creating a full volume $(t, \text{cmp}_x, \text{cmp}_y, hx, hy)$. Clapp (2005a) modified this approach to form a Common Azimuth dataset. The full volume of Clapp (2005b) is mapped into a Common Azimuth volume using AMO as part of the inversion.

In this paper, I build on the work of Clapp (2005a). I modify the data mapping operator to allow more mingling between hx volumes in the model space. In addition, each log-stretched frequency is done independently, allowing many more iterations to be applied economically. The methodology is applied on a marine dataset and compared to both a flex-binning and more standard AMO based approach.

THEORY

Estimating a regularly sampled common-azimuth volume $\mathbf{m}$ from our irregular input data $\mathbf{d}$ can be set up as a least squares inversion problem. The data consists of irregular traces in a 5-D space $(t, \text{cmp}_x, \text{cmp}_y, hx, hy)$. I want to apply a wave-number domain AMO operator (Biondi and Vlad, 2001) that works on regular cube, so the first step is to map the data onto a regular mesh. The operator $\mathbf{L}$ performs linear interpolation between the irregular dataspace and a regular 5-D mesh.

We want to create a common azimuth volume, specifically the zero azimuth volume, so we want to create a dataset where $hy = 0$. AMO provides a way to translate between different offsets. We can create an operator $\mathbf{Z}$ that sums over hy volumes that have been translated to $hy = 0$ using AMO. Unlike Clapp (2005a), we will also sum over a small range of hx. This additional summation allows for additional mixing of information in the five-dimensional space. We can define transforming from hx_1, hy_1 to hx_2, hy_2 using AMO as Z_{hx_1,hy_1,hx_2,hy_2}. We can define our hx sampling interval as d_{hx}, the number of samples as n_{hx}, and the first location as o_{hx}. Similarly our sampling hy is defined by n_{hy}, o_{hy}, and d_{hy}. Given Δhx samples we wish to sum over we can write an equation relating our domain m and range d through

$$m(ix) = \sum_{ix'=ix-\Delta x}^{ix+\Delta x} \sum_{iy=0}^{ny} Z_{ix' d_{hx}+o_{hx}, iy d_{hy}+o_{hy}, ix d_{hx}+o_{hx}, 0}(d(ix', iy)). \tag{1}$$

Where $m(ix)$ and $d(ix', iy)$ are 3-D cubes $(\mathbf{t}, \text{cmp}_\mathbf{x}, \text{cmp}_\mathbf{y})$.

Finally, we need to add in our regularization term. Generally, after NMO, our data should be smooth as a function of offset. By applying a derivative operator along the offset axis we can emphasize this smoothness and help fill in acquisition holes caused by data irregularity. We can improve this estimate even further by applying a derivative on cubes that have been transformed to the same offset using AMO[1] $\mathbf{D_h}$. We can write our objective function as

$$Q(\mathbf{m}) = ||\mathbf{d} - \mathbf{LZm}||^2 + \epsilon^2 ||\mathbf{D_h m}||^2 \tag{2}$$

[1]In this case AMO simplifies to Dip Move-out because it is being applied simply along the hx axis

where ϵ controls the importance of consistency along the offset axis. We can speed up the convergence of this problem by preconditioning the model with the inverse of our regularization operator. In this case, we replace taking the derivative of AMO cubes with performing causal integration of AMO cubes $\mathbf{C_h}$. Our new fitting goals then become

$$Q(\mathbf{p}) = ||\mathbf{d} - \mathbf{LZC_h p}||^2 + \epsilon^2 ||\mathbf{p}||^2 \tag{3}$$

where $\mathbf{m} = \mathbf{C_h p}$.

IMPLEMENTATION

A cost-effective implementation of (3) is challenging. The first question is whether to directly invert the matrix described by (3) by least-squares or use a reference model (Rickett, 2001; Biondi and Vlad, 2001) to approximate the implied Hessian by a diagonal matrix based on a reference model. A Hessian-based approach is easily parallelizable. The model can be broken along the hx axis. Each node is then given all of the data in $(hx_i - d_{hx}\Delta x, hx_i + d_{hx}\Delta x)$, where hx_i is the offset that a given node is creating.

If we do a full inverse then the obvious domain to parallelize the inversion is over frequency. In this case the model and data time axis is log-stretched and transformed into the frequency domain. The resulting model and data space are approximately three times the size of their time domain representation due to the oversampling necessitated by the log-stretch operation. In addition, both these volumes need to be transposed. To apply the log-stretch FFT operation, the natural ordering is for the time/frequency axis to be the inner axis while the inversion is more efficient with the time/frequency axis being the outer axis. An out-of-core transpose grows in cost with the square of the number of elements. For efficiency, I do a pre- and post-step parallel transpose of the data in conjunction with the transformation to and from the log-stretched frequency domain. I split the data long the cmp_y axis. Before the pre-step transpose I log-stretch and FFT the input data, I then do an out-of-core transpose of this smaller volume. I then collect the transposed data. The post-step operation is simply the inverse, transpose and then FFT and unstretch.

A second major problem is the number of iterations necessary for convergence. The causal integration and leaky integration are good preconditioners (fast convergence) but the AMO portion tends to slow the inversion. As a result many (20-100 iterations) are desirable. The global inversion approach described in Clapp (2005b) is Input/Output dominated. It also relies on hardware stability. Both of these factors make a frequency-by-frequency in-core inversion the non-ideal but better choice. The major drawback to a frequency-by-frequency approach is that the frequencies might converge at significantly different rates resulting in an image that is unrealistically dominated by certain frequency ranges (most likely the low). To minimize this problem, I stopped the inversion after a set reduction in the data residual for each frequency.

The final issue is the size of the problem. The domain of $\mathbf{L}$ is four-dimensional and can be quite large even for a relatively small model space. In addition, for a conjugate gradient approach we still must keep three copies of our data space (data, data residual, previous step data residual) and five copies of our model space (gradient, model, previous step, previous

step model residual, model residual). As a result, we need a machine with significant memory and/or must break the problem into patches in the $(\text{cmp}_x, \text{cmp}_y)$ plane.

REAL DATA EXAMPLE

I tested the methodology on a real 3-D marine dataset from the North Sea. Previous uses of AMO and common azimuth migration have resulted in noticeable acquisition footprint in the first 1300 meters (Biondi, 1999; Vaillant and Sava, 1999). I regularized, and then migrated, the volume using three different approaches. In the first approach I ignored the azimuth information to form my 4-D volume, I will refer to this methodology as the 'stack' approach. In the second approach I approximated the Hessian matrix by a diagonal based on a reference model, the 'reference' approach. And finally applied up to 120 conjugate iterations, 'inverse' approach. Figure 1 shows all three result. The top panel is the 'stack' approach, the center is the 'reference' approach, and the bottom panel is the 'inverse' approach. All the remaining figures will be of the same form.

Figure 2 compares a depth slice at 900 m. Note at 'A' what looks like noise on the 'stack' and 'reference' result, turns into a fault on the 'inverse' result At 'B' we see a steeply dipping reflector come into focus when we apply the 'reference' approach. The acquisition footprint visible at 'C' diminishes with the 'reference' approach, and is almost completely absent in the 'inverse' result. At a depth of 1360 m (Figure 3) we can see similar improvements. At 'A' we see fault reflection that is not visible on the 'stack' result, barely visible on the 'reference' result become very evident on the 'inverse' result. At 'B' we see significant acquisition footprint in the 'stack' result, it is reduced significant in the 'reference' result, and in the 'inverse' result we begin to see additional fine featured geology appear. At 'C' we a portion of fault in the 'stack' result, continuous segment in the 'reference' result, and the entire fault reflection in the 'inverse' result. Figure 4 shows a cross-line located at 7200m. Note the fault reflection at 'A' that is barely visible in the 'stack' result appear in the 'reference' result, and become coherent in the 'inverse' result. Note the small faults at 'B' that are not visible in the 'stack' or 'reference' result become evident in the 'inverse' result. Figure 5 shows a cross-line at 8200m. Note the small faults become much more evident as we progress from the 'stack' to the 'inverse' result. At 'B' we see the migration artifacts dramatically decrease as we move from the 'reference' to the 'inverse' result.

Figure 6 shows an inline section at 3100m. Note the steeply dipping reflectors that are not visible at 'A' in the 'stack' result come into focus in the inverse result. At 'B' we see a peak that isn't visible in either the 'stack' or 'reference' result appear in the inverse result. At 'C' we see a package of reflectors that are incoherent in the 'stack' result become clearer as we move to the 'reference' and 'inverse' result. Figure 7 shows an inline section location at 3960m. At 'A' the complex folding above the salt intrusion come into focus in the 'inversion' result. The set of reflectors above the salt come into focus as we advance to more sophisticated techniques at 'B'. At 'C' we see the salt reflection come into focus as we move to the 'reference' and 'inverse' approach.

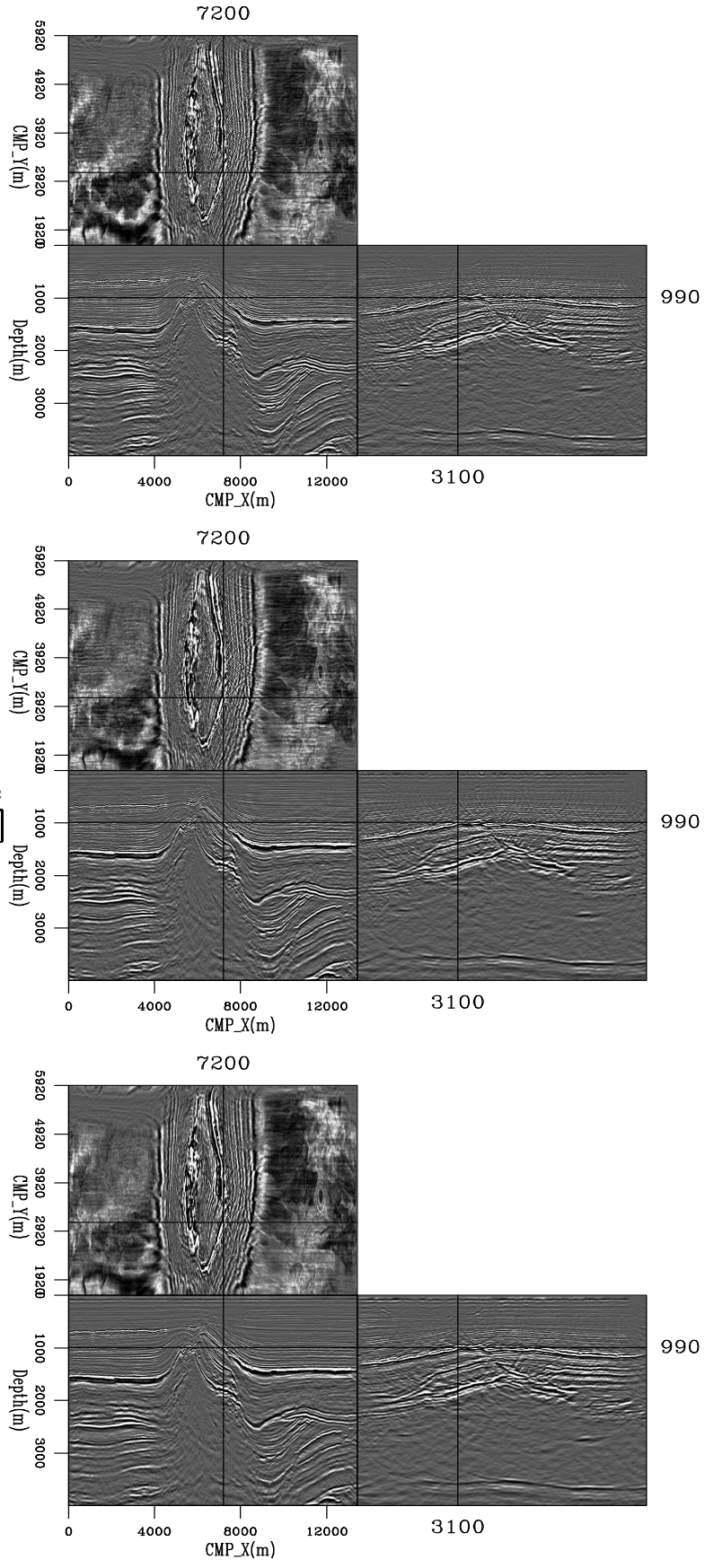

Figure 1: The top panel is the 'stack' approach, the center is the 'reference' approach, and the bottom panel is the 'inverse' approach. bob1-cube [CR,M]

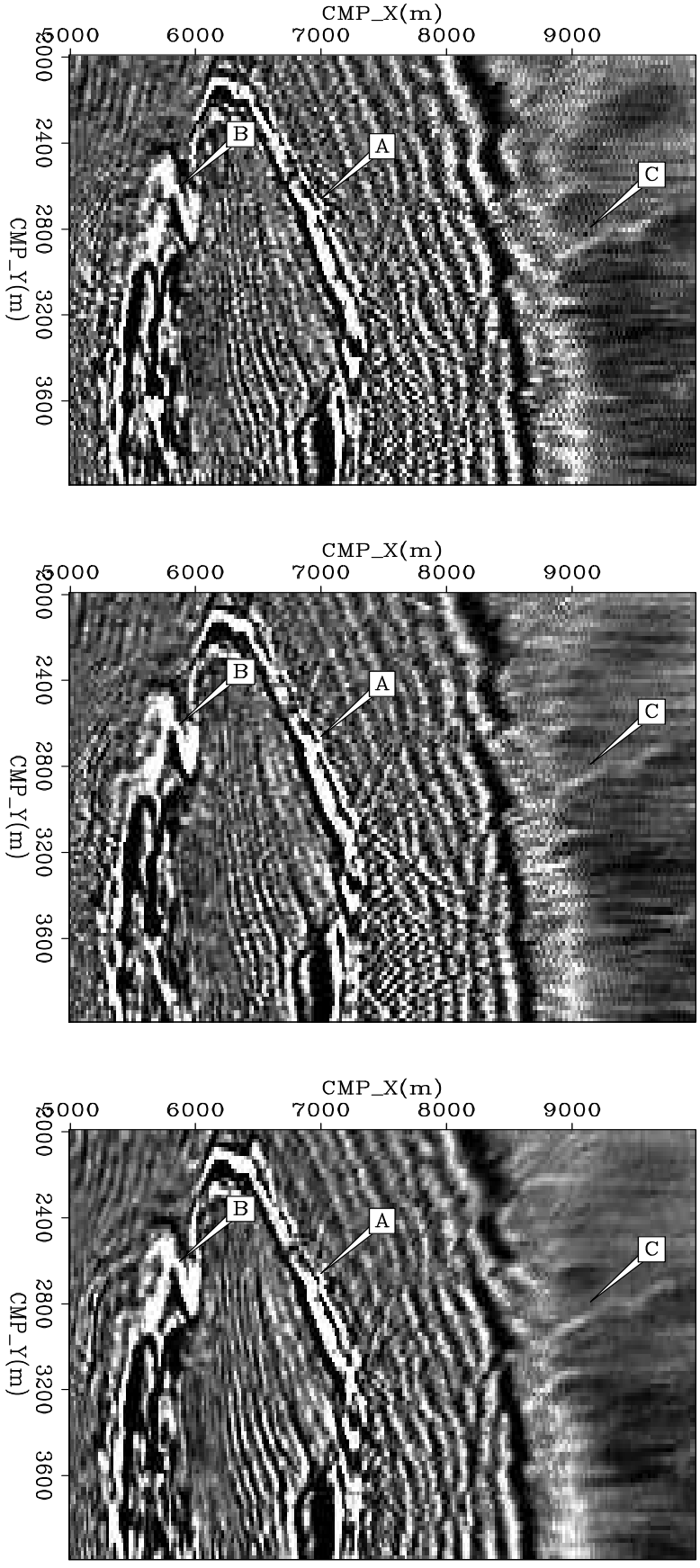

Figure 2: The top panel is the 'stack' approach, the center is the 'reference' approach, and the bottom panel is the 'inverse' approach. Note at 'A' what looks like noise on the 'stack' and 'reference' result, turns into a fault on the 'inverse' result At 'B' we see a steeply dipping reflector come into focus when we apply the 'reference' approach. The acquisition footprint visible at 'C' diminishes with the 'reference' approach, and is almost completely absent in the 'inverse' result. bob1-depth1 [CR,M]

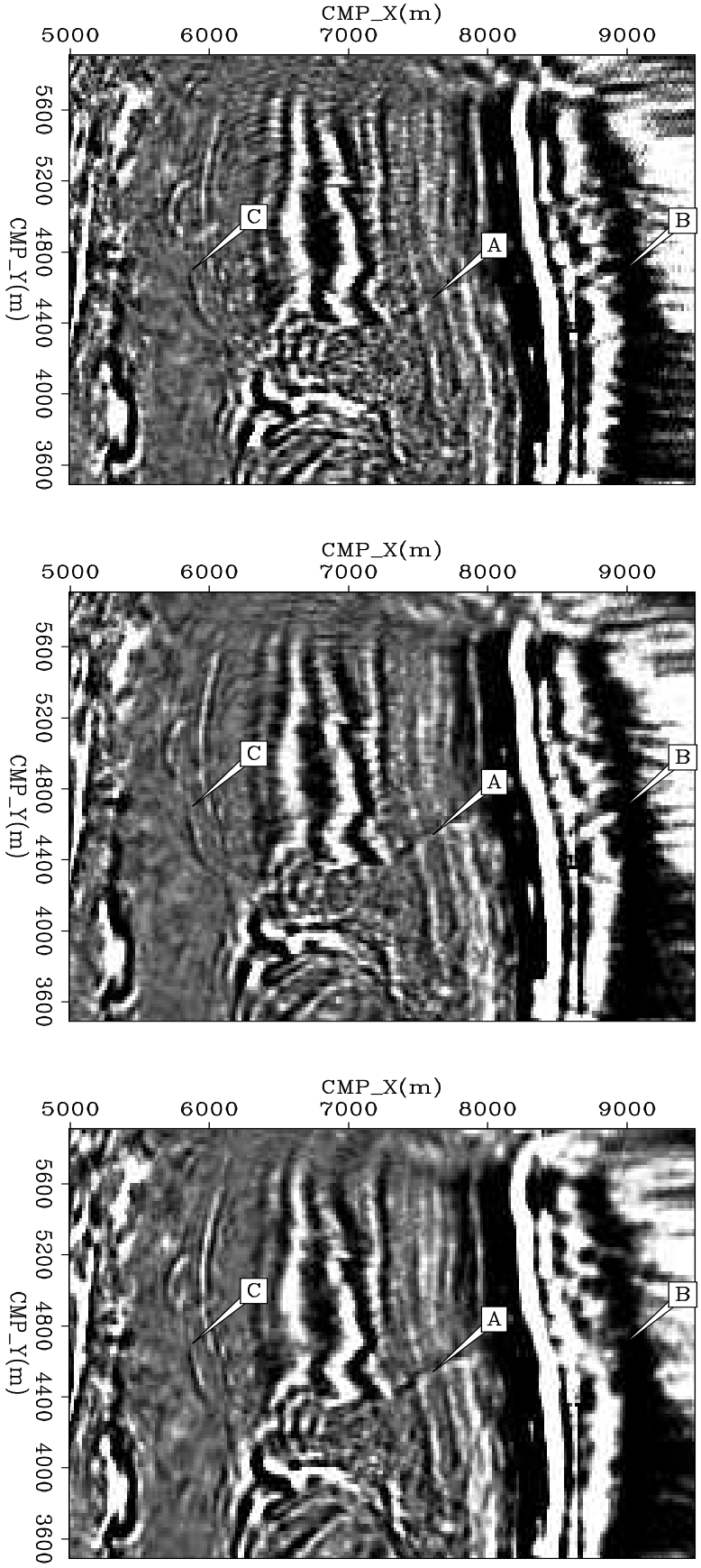

Figure 3: The top panel is the 'stack' approach, the center is the 'reference' approach, and the bottom panel is the 'inverse' approach. At 'A' we see fault reflection that is not visible on the 'stack' result, barely visible on the 'reference' result become very evident on the 'inverse' result. At 'B' we see significant acquisition footprint in the 'stack' result, it is reduced significant in the 'reference' result, and in the 'inverse' result we begin to see additional fine featured geology appear. At 'C' we a portion of fault in the 'stack' result, continuous segment in the 'reference' result, and the entire fault reflection in the 'inverse' result. bob1-depth2 [CR,M]

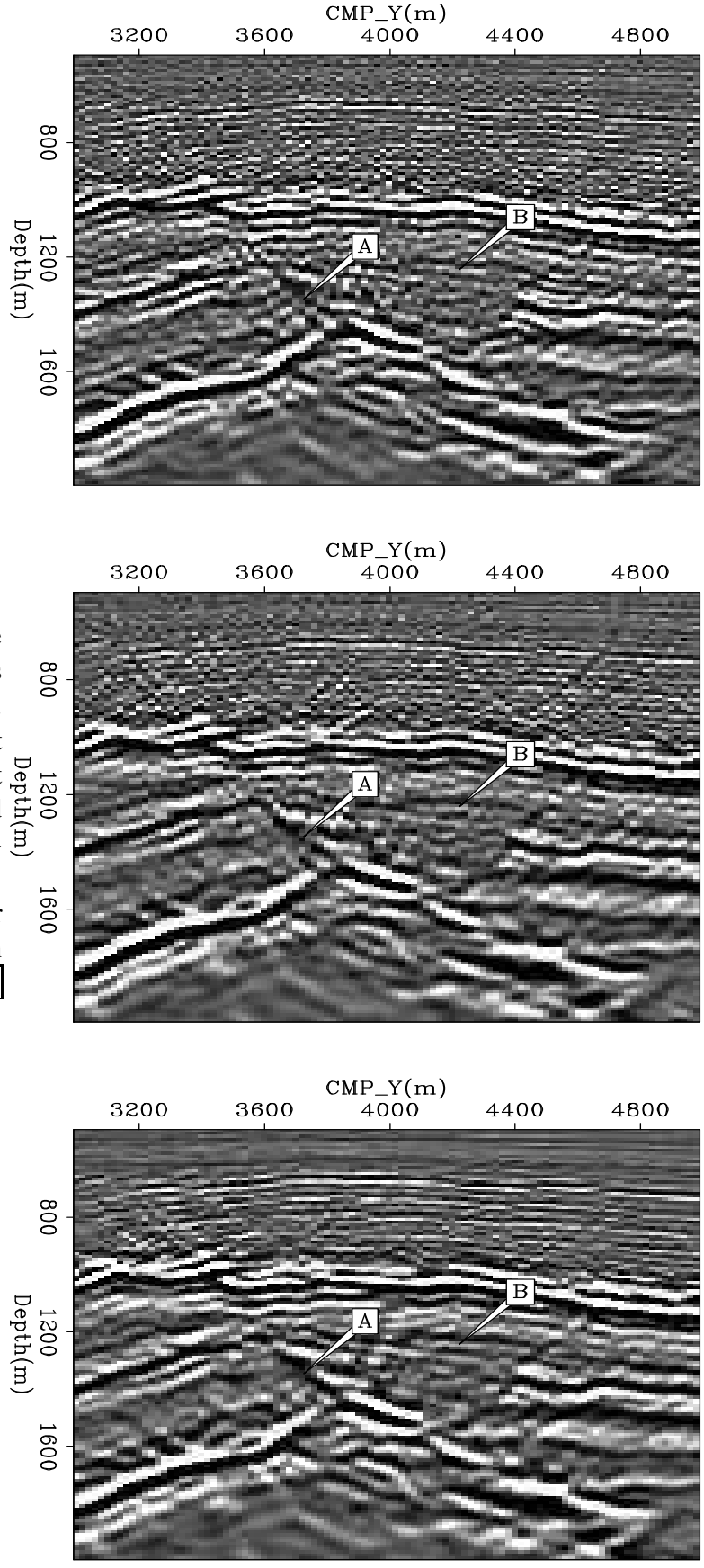

Figure 4: The top panel is the ‘stack’ approach, the center is the ‘reference’ approach, and the bottom panel is the ‘inverse’ approach. All three figures show a cross-line located at 7200m. Note the fault reflection at ‘A’ that is barely visible in the ‘stack’ result appear in the ’reference’ result, and become coherent in the ‘inverse’ result. Note the small faults at ‘B’ that are not visible in the ‘stack’ or ‘reference’ result become evident in the ‘inverse’ result. bob1-xline1 [CR,M]

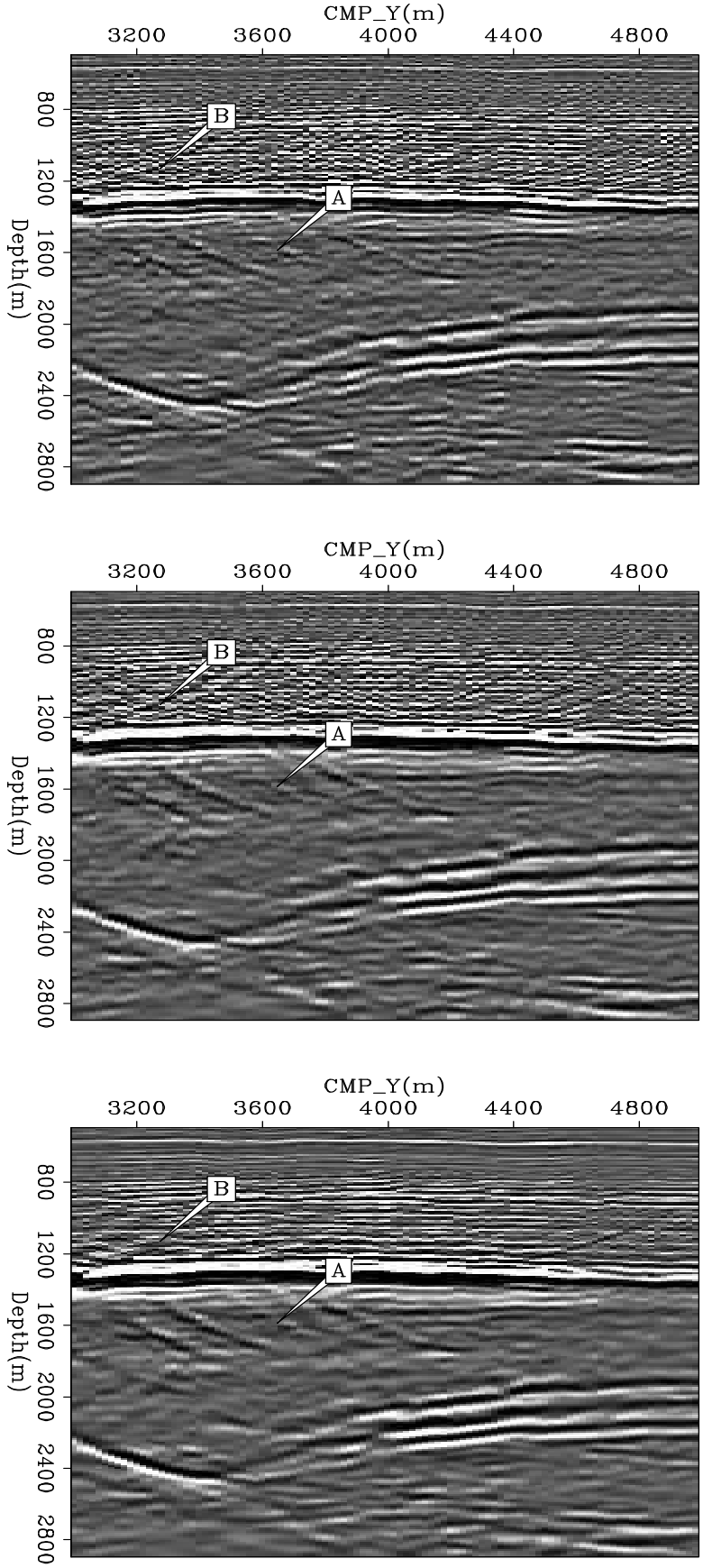

Figure 5: The top panel is the 'stack' approach, the center is the 'reference' approach, and the bottom panel is the 'inverse' approach. All three figures show a cross-line located at 7200m. Note the small faults become much more evident as we progress from the 'stack' to the 'inverse' result. At 'B' we see the migration artifacts dramatically decrease as we move from the 'reference' to the 'inverse' result. bob1-xline2 [CR,M]

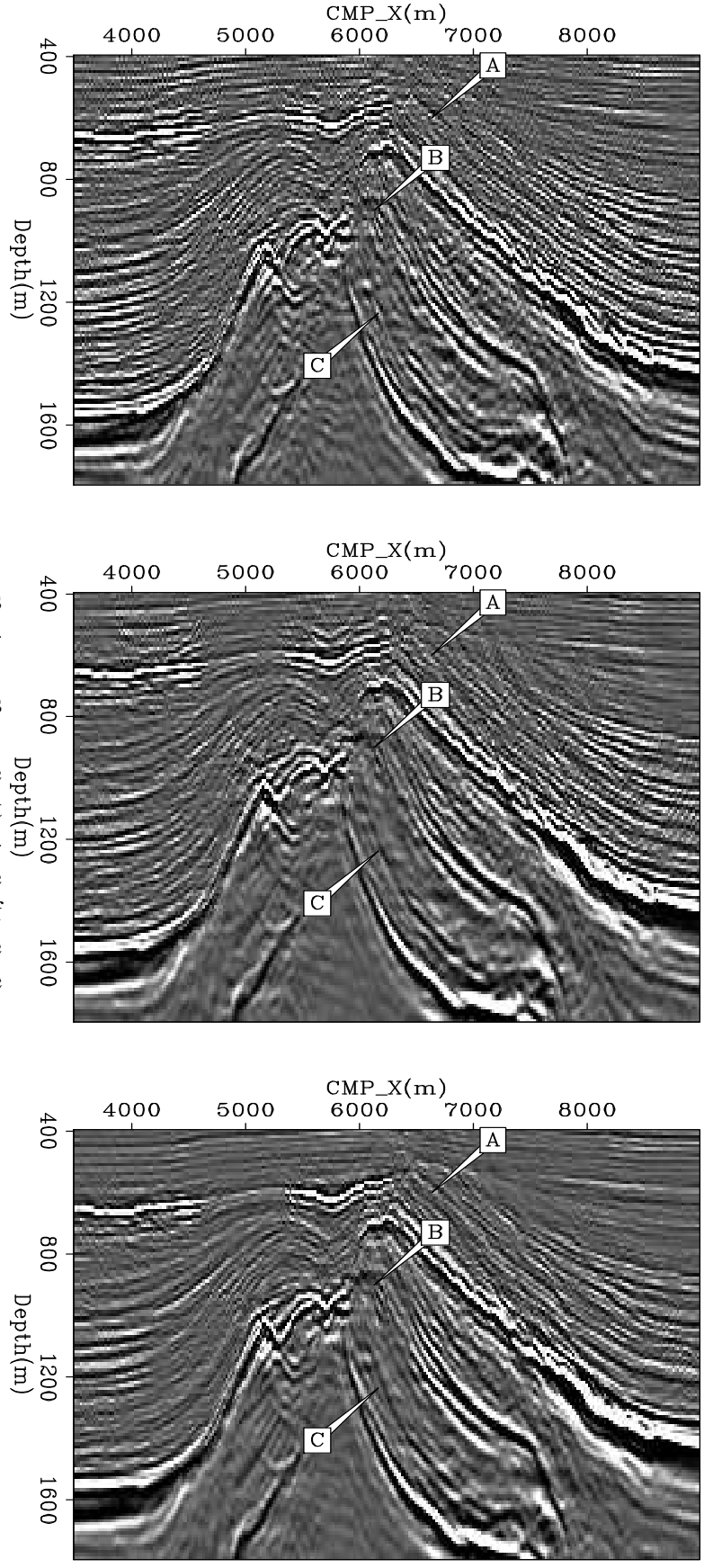

Figure 6: The top panel is the 'stack' approach, the center is the 'reference' approach, and the bottom panel is the 'inverse' approach. All three figures show a in-line located at 3100m. Note the steeply dipping reflectors that aren't visible at 'A' in the 'stack' result come into focus in the inverse result. At 'B' we see a peak that isn't visible in either the 'stack' or 'reference' result appear in the inverse result. At 'C' we see a package of reflectors that are incoherent in the 'stack' result become clearer as we move to the 'reference' and 'inverse' result. bob1-iline1 [CR,M]

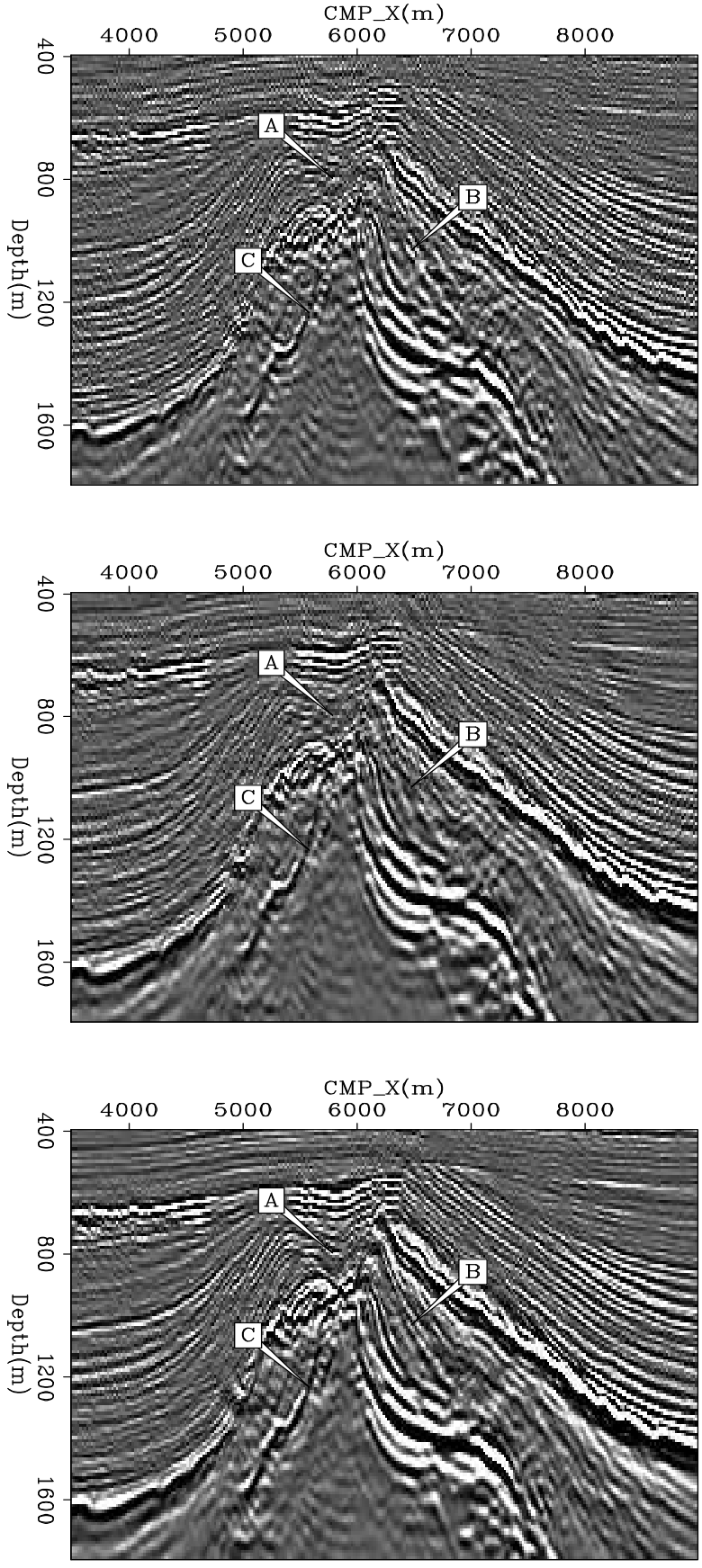

Figure 7: The top panel is the 'stack' approach, the center is the 'reference' approach, and the bottom panel is the 'inverse' approach. All three figures show a in-line located at 3960. . At 'A' the complex folding above the salt intrusion come into focus in the 'inversion' result. The set of reflectors above the salt come into focus as we advance to more sophisticated techniques at 'B'. At 'C' we see the salt reflection come into focus as we move to the 'reference' and 'inverse' approach. bob1-iline2 [CR,M]

CONCLUSION

I introduced an inversion method to produce a dataset appropriate for common azimuth migration. The inversion problem uses AMO to both map the data to a constant $hy = 0$ and as part of regularization operator to assure consistency between $(\text{cmp}_x, \text{cmp}_y, hx)$ cubes.

ACKNOWLEDGMENTS

I would like to thank TotalFinaElf for providing the data used in this paper.

REFERENCES

Biondi, B. and I. Vlad, 2001, Amplitude preserving prestack imaging of irregularly sampled 3-D data: SEP–**110**, 1–18.

Biondi, B., S. Fomel, and N. Chemingui, 1998, Azimuth moveout for 3-D prestack imaging: Geophysics, **63**, no. 2, 574–588.

Biondi, B. L., 1999, 3-D Seismic imaging: Stanford Exploration Project.

Chemingui, N., 1999, Imaging irregularly sampled 3D prestacked data: SEP–**101**.

Clapp, R. G., 2005a, Amo inversion to a common azimuth dataset: SEP–**123**.

Clapp, R. G., 2005b, Data regularization: Inversion with azimuth move-out: SEP–**120**, 187–196.

Duquet, B. and K. J. Marfurt, 1999, Filtering coherent noise during prestack depth migration: Geophysics, **64**, no. 4, 1054–1066.

Fomel, S., 2001, Three-dimensional seismic data regularization: Ph.D. thesis, Stanford University.

Prucha, M. L., R. G. Clapp, and B. Biondi, 2000, Seismic image regularization in the reflection angle domain: SEP–**103**, 109–119.

Rickett, J., 2001, Spectral factorization of wavefields and wave operators: Ph.D. thesis, Stanford University.

Ronen, S. and C. L. Liner, 2000, Least-squares DMO and migration: Geophysics, **65**, no. 5, 1364–1371.

Vaillant, L. and P. Sava, 1999, Common-azimuth migration of a North Sea dataset: SEP–**102**, 1–14.